Evaluating Angle of Arrival and Distance with Ultra WideBand Technology for Indoor Localization

Fabio Mavilia, Francesco Furfari, Paolo Barsocchi and Michele Girolami
Italian National Council of Research, ISTI-CNR, Pisa, Italy
Email: {name.surname}@isti.cnr.it

***Abstract*—Several radio-frequency technologies have been investigated to develop accurate indoor localization systems, each offering distinct techniques for estimating a target's position in indoor environments. Among them, the Ultra-WideBand (UWB) technology is a promising approach because it can estimate the distance and angle between a tag and an anchor. In this work, we evaluate the performance of a commercial UWB kit with a systematic data collection campaign. We gather data in a realistic setting, comparing estimated and actual Angles of Arrival (AoA) and distances. Results highlight that, while the system performs reliably in most scenarios, a few instances reveal noticeable deviations from the Ground Truth (GT) data.**

***Index Terms*—UWB, Time of Flight, Angle of Arrival, Indoor Localization**

I. Introduction

Recent years have seen a proliferation of techniques and technologies for designing and evaluating indoor localization systems [1], [2]. The well-known RSS (Received Signal Strength, [3]) indicator has been replaced or integrated with more advanced RF-based measures, such as CSI (Channel State Information) and AoA/AoD (Angle of Arrival and Departure). In particular, the use of MIMO antennas enables the estimation of the angle between an emitter and a receiver. Currently, two commercial RF-technologies offer such possibilities: Bluetooth 5.1 Direction Finding [4], [5], [6] and Ultra-WideBand [7]. Specifically, UWB-based systems demonstrate robustness in indoor localization scenarios due to the adopted frequencies (e.g., 6.5 GHz and 8 GHz), which are less susceptible to signal attenuation caused by obstacles. Additionally, UWB chipsets have been integrated with commercial smartphones (such as Google Pixel 6/7 Pro, Apple iPhone 11+, etc.), enabling smartphones to self-localize.

In this study, we investigate the capabilities of UWB technology to develop an indoor localization system. Specifically, we assess the performance of a commercial off-the-shelf (COTS) product, the QM33120WDK1 kit by Qorvo, in a real-world setting characterized by a spacious indoor environment. Our experimental setup involves deploying one tag and one anchor node and collecting data from 81 predetermined testing locations arranged in a regular 6 m $\times$ 6 m grid. Both the anchor and the tag are mounted on tripods, with the anchor's height varying from 120 cm to 230 cm above the ground.

The anchor node records the estimated Angle of Arrival (AoA) on the azimuth plane and the distance from the tag at a frequency of 5 Hz, resulting in approximately 40,000 collected samples over 2.5 hours of data collection. Interestingly, the adopted hardware combines two techniques. On the one hand, the AoA is obtained with a MIMO antenna, while the distance is obtained with the TDoA (Time Difference of Arrival) technique. Additionally, we obtain accurate Ground Truth annotations, providing the actual angle and distance measurements for every testing location.

To evaluate the accuracy of the UWB kit data (AoA and distance), we compute the Mean Absolute Error (MAE) between the ground truth and estimated values. Our experimental findings reveal that the MAE of the AoA increases only in peripheral regions where the angle between the tag and anchor is wide (e.g. 60°- 80°). Under such conditions, we obtain MAE values ranging up to 20°. Concerning the estimated distance between the tag and the anchor, we observe errors of up to 30 cm. We further discuss how to utilize a commercial UWB kit to deploy and test an indoor localization system in a real-world setting.

II. Related Work

In this section, we provide a review of existing works leveraging UWB technology, focusing on: (i) publicly available datasets for indoor localization, and (ii) real-world UWB-based localization systems.

The authors of [8] describe a dataset obtained with UWB sensors collecting Channel Impulse Response samples. The adopted hardware is based on COTS equipment. The dataset includes about 1.6 hours of annotated measurements collected in a residential environment. Its primary purpose is passive indoor target tracking, with potential for UWB-based Human Activity Recognition (HAR) involving three postures: sitting, standing, and walking. In [9], the authors introduce a dataset based on Bluetooth Low Energy (BLE) and UWB technology for motion capture systems. The adopted hardware is based on the OptiTrack kit and the following covered application scenarios: walking and trolley. The data collected include AoA, RSSI, and (x,y)-coordinated data estimated with both BLE and UWB technologies.

The authors of [10] propose an indoor positioning system utilizing fixed AoD tags. This system relies on the IEEE 802.15.4z UWB standard and achieves an accuracy of 5° for AoD angle estimation within a range of $-30°$ to 30°. Notably, the system employs custom-designed tags based on the Qorvo SoC DW3120, rather than commercially available options. In [11], Margiani et al. present a sensor node utilizing the Qorvo DW3220 for indoor positioning. Their system achieves centimeter-level distance accuracy and an impressive average AoA accuracy of 2.4° under specific operating conditions, specifically in the range of $-45°$ to 45°. Finally, the authors of [12] explore a deep convolutional neural network for AoA estimation using a regression approach. Their experimental setup involved a challenging environment with noise and multipath effects. The proposed solution achieves a 99th percentile error of 2.8° for AoA estimation in the entire range of $-90°$ to 90°.

In summary, research on AoA estimation using UWB radios has explored two main approaches: traditional rule-based techniques such as MUSIC and PDoA, and machine learning (ML)-based methods. Overall, ML-based solutions have been shown to outperform the classic PDoA approach in the range of $\pm 90°$ because the nonlinearity of the PDoA suffers from extreme angles. However, it is important to note that these conclusions are valid only when the neural network has been trained and tested in identical environments.

III. Principles of the UWB positioning method

A. Measuring the Distance

The distance measurement between UWB devices, using the Two-Way Ranging (TWR) method, is simplified because each UWB device can utilize its independent clock-based timestamp. This eliminates the need for a separate external synchronization process. The TWR method is categorized into two main approaches: Single-Sided Two-Way Ranging (SS-TWR) and Double-Sided Two-Way Ranging (DS-TWR). SS-TWR is the simpler approach, requiring only two message exchanges to calculate the Time of Flight (ToF). The anchor node initiates the process by transmitting a message to the tag node and records the transmission start time, denoted as t_1 in Fig. 1a. Upon receiving and processing the signal, the tag node responds with a message. Finally, the anchor node records the timestamp, t_2, upon receiving the response and can then calculate the ToF.

The principle of DS-TWR operation is illustrated in Fig. 1b. The tag node initiates the process by transmitting a 'Poll' message and records the timestamp t_1. The anchor receives the message, records the timestamp t_2 and then sends a Response message. Finally, the tag receives the Response message, records the timestamp t_3, and sends the 'Final' message. In indoor positioning systems, the DS-TWR method is generally preferable because of its scalability advantages. DS-TWR involves multiple communication rounds between the UWB tag and anchor, which facilitates a more precise distance estimation. While SS-TWR is conceptually simpler,

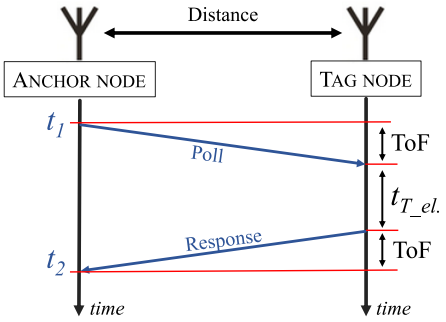

(a) Message exchange principle in the SS-TWR based method.

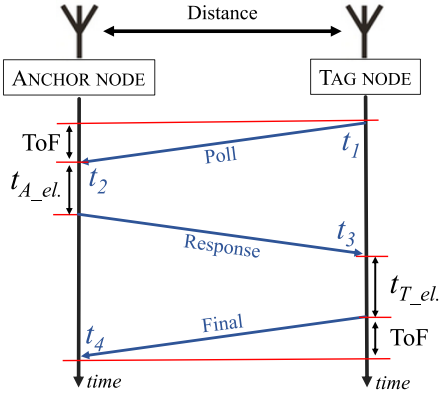

(b) Message exchange principle in the DS-TWR based method.

Fig. 1: The TWR distance measurement method used in UWB standards.

it can encounter difficulties when scaling to multiple tags or anchors. These challenges can include interference and synchronization issues. Consequently, for seamless and reliable implementation of indoor positioning with multiple tags or anchors, the DS-TWR method is the preferred choice.

B. Estimating the Angle of Arrival

To determine the angle of arrival of the signal, the TDoA and PDoA methods can be employed. Both methods require a receiver equipped with at least two antennas. The TDoA indicates the time difference of the same signal arriving at the two antennas. Given the typical spacing between antennas, which is usually half a wavelength or less, the TDoA typically falls below 1 ns. In contrast, the PDoA quantifies the difference in the signal phase, caused by an additional travel distance, denoted as t in Fig.2, between the first antenna and the same signal arriving at the second antenna. The angle of arrival ϕ exhibits a close relationship with the PDoA and can be calculated using the geometric approach outlined in Fig.2, following the equation:

$$\phi = \arccos\left(\frac{\lambda\gamma}{2\pi d}\right) \tag{1}$$

where γ is the PDoA, λ is the wavelength of the signal and d is the distance between the antennas. Systems relying

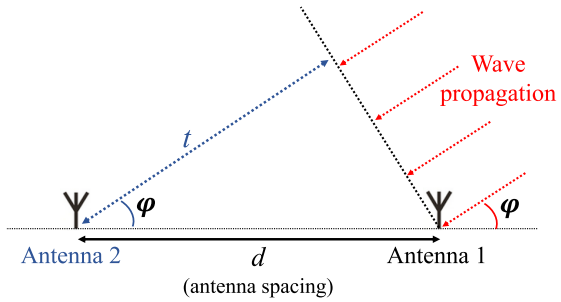

Fig. 2: AoA computation based on the geometry of the dual antenna.

on dual-antenna receivers are suitable for detecting signals travelling along a Line-of-Sight (LOS) path. However, in real-world indoor environments, incoming signals often experience multipath effects, arriving from various directions. Consequently, employing a compensation algorithm or a system equipped with more than two antennas, can prove advantageous in mitigating these sources of inaccuracy.

Furthermore, due to the effect known as front-back ambiguity [13], angle measurements are limited to a range of $\pm 90°$. This limitation arises from the inability to differentiate between signals arriving from the 'front' and the 'back' of the module. To address this limitation, the receiver is typically positioned facing a wall or an inaccessible area.

IV. Experimental Settings

We now outline the setup of our experimental data collection campaign. First, we detail the hardware kit utilized. Second, we provide a comprehensive description of the experimental environment.

A. The hardware kit

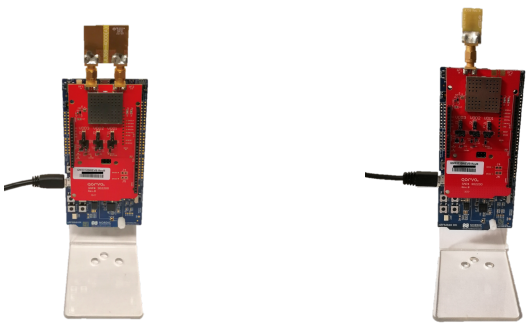

(a) Anchor node. (b) Tag node.

Fig. 3: The hardware kit used for data collection.

Our data collection campaign relies on the QM33120WDK1 development kit by Qorvo[1]. This kit complies with the FiRa PHY/MAC specification and adheres to the standards IEEE 802.15.4-2020 and IEEE 802.15.4z-2020 BPRF. Notably, the platform offers significant capabilities for developing and implementing TWR, PDoA, and AoA-based solutions in wireless networks. As shown in Fig.3, the kit consists of two evaluation boards with the following features:

- one daughter board, based on the QM33120W UWB transceiver and the JL359 directional dual-antenna. It can measure both the angle of arrival and the distance and acts as the anchor node in the AoA system (Fig.3a).
- one daughter board, which embeds the QM33110W UWB transceiver and the JL159 omni-directional single-antenna. It can calculate distance and it acts as the tag node in the AoA system (Fig.3b).

Both antennas operate on UWB channels 5 and 9, corresponding to 6.5 GHz and 8 GHz, respectively. The boards are connected to the pre-programmed Nordic nRF52840 evaluation board for debugging and flashing via a USB interface. Additionally, the boards are mounted on plastic stands that hold them in a vertical position, as illustrated in Fig.3.

The nodes are equipped with dedicated firmware provided by Qorvo. The firmware enables the estimation of two key-values:

- the AoA on the azimuth plane between the tag and the anchor;
- the distance, expressed in centimeters, between the tag and the anchor.

The anchor and the tag are connected to a Raspberry Pi board, which logs each received message along with its corresponding timestamp.

B. The experimental dataset

The experiments are conducted in a wide indoor room at our research institute, CNR-ISTI, located in Pisa, Italy. The experimental area is a square of 6 m $\times$ 6 m, located within a larger empty room of 110.4m^2 (13.8 m $\times$ 8.0 m). The ceiling is 3.1 m in height and the floor is covered in 60$\times$60cm regular tiles. A 2-D visualization of the experimental layout is shown in Fig.4. We deploy the anchor node, held by a tripod, at position (x=0, y=0). It is positioned parallel to the wall. We test two different heights:

- Setting 1: the anchor lies 120 cm above the ground;
- Setting 2: the anchor lies 230 cm above the ground;

The tag is mounted on a tripod at a fixed height of 120 cm, oriented toward the anchor. For each of the two settings, we position the tag in 81 locations, according to a regular grid, as shown in Fig.4.

The 81 test locations allow us to collect data across a variety of angles and distances between the tag and the anchor. Specifically, the range of the experimented angle varies from $-76°$ (location `-240,60`) to $76°$ (location `240,60`), while the range of distances ranges from 60 cm (setting 1, location `0,60`) to 6.01 m (setting 2, locations `240,540` and `-240,540`).

[1]https://www.qorvo.com/products/p/QM33120WDK1

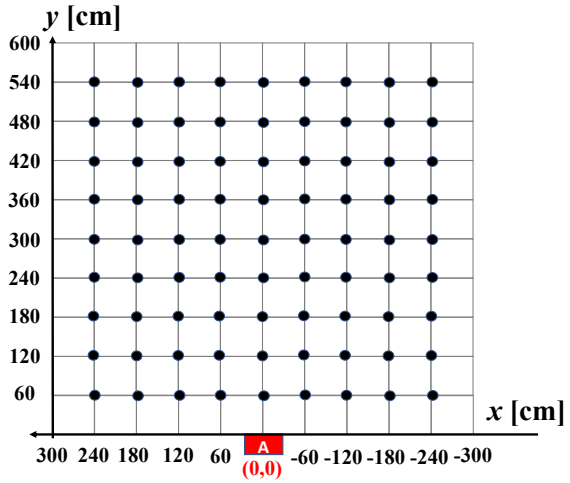

Fig. 4: A 2D visualization of the experimental map.

TABLE I: Data format of log data.

Epoch Time	Angle of Arrival	Distance

We collect data for 1 minute at each of the 81 positions, for a total recording time exceeding 2.5 hours. The dataset consists of the log data produced by the anchor node and a Ground Truth annotation. Concerning the log data, Table I reports the collected information. Concerning the Ground Truth, we keep track of the following information:

- the start time and end time for each of the 81 locations;
- the actual AoA on the azimuth plane between the tag and the anchor;
- the actual distance between the tag and the anchor.

This information allows us to evaluate the accuracy of the estimated angles and distances in each location, as reported in Section V.

V. Experimental Results

In this section, we evaluate the quality of the data provided by the anchor node by estimating two key metrics: the AoA on the azimuth plane and the distance to the tag. To this end, we compare these estimates with the GT annotations by calculating the mean absolute error (MAE). For instance, regarding the AoA on the azimuth plane, the MAE is obtained as follows:

$$MAE_{\phi} = \frac{\sum_{i=1}^{n} |\phi_i - \hat{\phi}_i|}{n} \quad (2)$$

where ϕ represents the actual AoA and $\hat{\phi}$ the anchor's estimated angle.

The results for the AoA on the azimuth plane are shown in Fig. 5. The figure presents the results for the two adopted settings of anchor A: z=120 cm (Setting 1) and z=230 cm (Setting 2). The error bar on the right side of Fig. 5 shows the error introduced by the anchor, expressed in degrees. Concerning Setting 1, we observe a significant increase in the MAE at the periphery, such as at locations: $(240, 60)$ and $(-240, 60)$. Such regions correspond to the maximum AoA between the tag and the anchor, leading to high inaccuracy. Conversely, the MAE remains relatively stable in most other areas of the experimental room. Notably, in Setting 1, both the anchor and the tag are positioned at the same height of 120 cm from the ground.

For Setting 2, we observe a pattern slightly different from that of Setting 1. More specifically, the MAE tends to increase *close* to the anchor's location: $(0, 60)$, $(60, 60)$ and in peripheral locations, such as $(-240, 60)$. In this setting, the anchor is positioned higher relative to the tag, resulting in a noticeable error close to the anchor's location.

We further analyze the MAEs obtained with Setting 1 and 2 by showing how the MAEs on the azimuth plane vary with respect to the actual angle, as reported in Fig. 6. The figure displays the results for Setting 1 as a blue dashed line and Setting 2 as a red dashed line. The two curves are obtained by interpolating the MAE values (81 samples, one for each location) with a polynomial fit. The curves clearly indicate that the MAE tends to increase at the periphery, such as for locations corresponding to $(80°, 40°)$ and $(-40°, -80°)$. Moreover, we observe that the MAE remains relatively stable when computed for angles between $40°$ and $-40°$ (e.g. $5°$ error for Setting 2). Table II reports the 50th, 75th, and 90th percentiles of the AoA error for both settings.

We evaluate the estimated distance between the tag and anchor using the MAE as well. Fig. 7 shows the resulting heatmaps for both Setting 1 and 2. As a general consideration, we observe a greater MAE with Setting 1 than with Setting 2. In the first case, in some regions, the estimated distance deviates from the GT, as seen at locations $(-120, 180)$ and $(-60, 300)$. However, the error in these locations remains within 30 cm. Conversely, the computed error with Setting 2 is always below 15 cm. Nonetheless, both settings achieve a sub-meter error, which is a promising result for indoor localization.

Similar to the AoA analysis, we further analyze how the MAE for distance varies with the actual distance, as shown in Fig. 8. The blue dashed line reports the results for Setting 1, while the red dashed line represents Setting 2. As before, we interpolate the MAEs (81 samples) using a polynomial fit. The graph reveals an interesting pattern for both of the settings: the MAE tends to decrease as the distance increases. This trend is particularly evident in Setting 1, where the MAE ranges from 24 cm (no distance between the anchor and the tag) to 5 cm (a distance of 6 meters between the anchor and the tag). Table II reports the 50th, 75th, and 90th percentiles of the distance error for both settings.

VI. Discussion and Conclusions

The experiments outlined in this study provide valuable insights into UWB-based indoor positioning. Overall, user position can be estimated through AoA, ToF, or hybrid methods. The optimal technique depends on factors like the

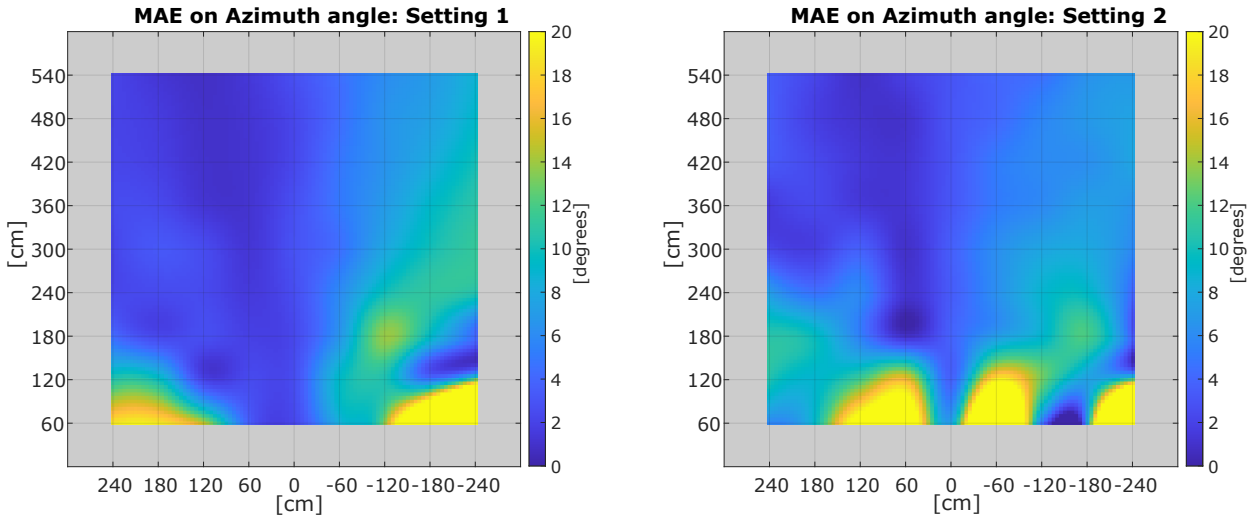

Fig. 5: Heatmap of the MAE for the azimuth angle with anchor A at z=120 cm (Setting 1) and at z=230 cm (Setting 2).

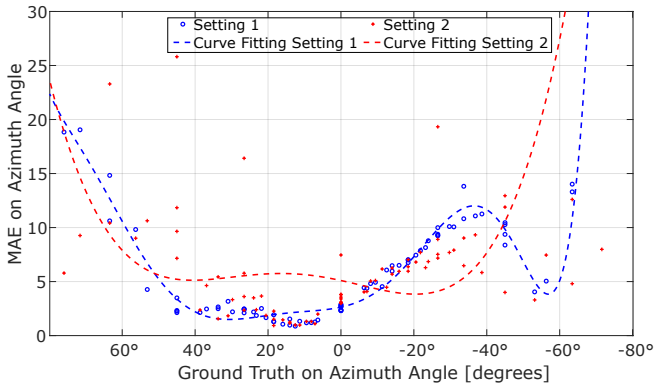

Fig. 6: MAE for the azimuth angle with respect to the actual angles.

TABLE II: Percentiles of AoA and distance error for Setting 1 (anchor and tag placed at 120 cm above the ground) and Setting 2 (anchor located 230 cm above the ground and tag at 120 cm above the ground).

		Error Percentile		
		50th	75th	90th
AoA [degrees]	**Setting 1** (anchor low)	**4.2°**	**9.3°**	**12°**
	Setting 2 (anchor high)	5.7°	7.7°	12.2°
Distance [cm]	Setting 1 (anchor low)	8.5	11.3	15.2
	Setting 2 (anchor high)	**4.1**	**6.2**	**8.2**

number of anchors, availability of height information, and whether planar or 3D positioning is required.

When using a single anchor node, the tag's height is crucial for accurate planar coordinate estimation. Knowing the height difference between tag and anchor enables the use of spherical coordinates (distance, azimuth, elevation) to derive x, y, and z. If the tag height is unknown and two anchors are available, planar coordinates can be determined by intersecting the signal arrival angle lines. To estimate the z coordinate, distance information (ToF) is required.

With three anchors, a more accurate 2D position can be estimated using signal arrival angles. Alternatively, 3D positioning can be achieved via trilateration using ToF-based distances. When using three or more anchors, multilateration based on distance is recommended, as angular errors converted to meters are generally larger than those from ToF-based estimation. For instance, a 5° AoA error at a 6 m distance translates to a 52 cm error, whereas a ToF error at the same distance is approximately 5 cm (as reported in Fig. 8 at 600 cm).

However, AoA estimation can be advantageous at close distances. At 60 cm, the AoA error is 5 cm (as shown in Fig. 6 at 0°), while the ToF has a 20 cm error (Fig. 8 at 60 cm). Geometric transformations from AoA errors to meters have less impact at close distances. Conversely, ToF requires precise time discrimination for short distances, which can affect positioning accuracy. As a result, positioning accuracy may be affected, as seen in the example of estimating the position at coordinate points `(0, 60, 120)`. In Setting 1, where the anchor is positioned only 60 cm from the tag, the estimate is worse than that in Setting 2, where the anchor is raised to a distance of 125 cm. Thus, for ToF-based techniques, greater placement of anchors yields better results.

On the other hand, AoA measurements are more stable within an angular range of 60° to −60°, when the anchor's azimuthal plane is at the same height as the tag. The maximum errors in this range are approximately 10°. Raising the anchor and its azimuthal plane to 230 cm in Setting 2 leads to more outliers, with errors ranging from 15° to 25°.

In the near future we plan to investigate two lines of research. First, we intend to gather and share an expanded dataset with the research community to facilitate the testing of algorithms and solutions for indoor localization. Second,

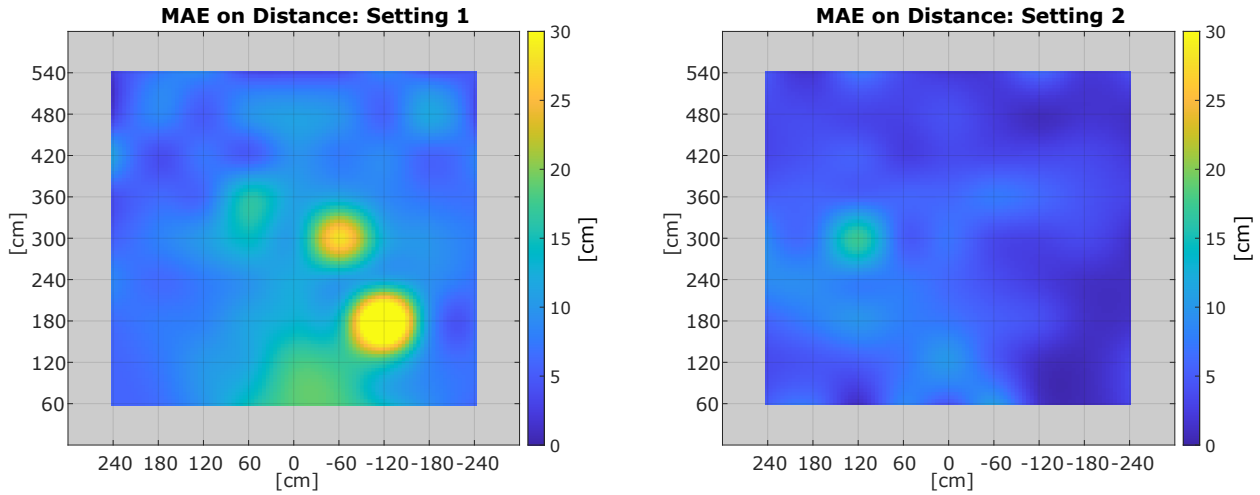

Fig. 7: Heatmap of the MAE of the distance between the anchor and the tag, with anchor A at z=120 cm (Setting 1) and at z=230 cm (Setting 2).

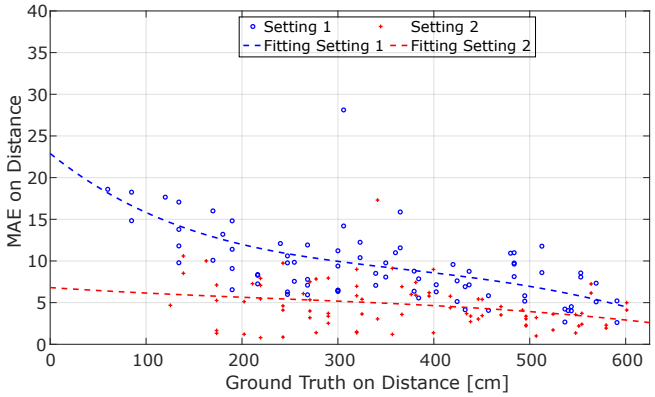

Fig. 8: MAE of the distance with respect to the actual distances.

we plan to analyze the collected data to evaluate and refine indoor localization algorithms that combine distance and AoA estimation.

Acknowledgment

This work is partially funded by European Union - Next Generation EU, in the context of The National Recovery and Resilience Plan, Investment Partenariato Esteso PE8 ”Conseguenze e sfide dell’invecchiamento”, Project Age-IT, CUP: B83C22004800006 and by STRIVE Project CUP: B53C22010110001 by MUR ministry.

References

[1] F. Zafari, A. Gkelias, and K. K. Leung, “A survey of indoor localization systems and technologies,” *IEEE Communications Surveys & Tutorials*, vol. 21, no. 3, pp. 2568–2599, 2019.

[2] M. Girolami, F. Mavilia, and F. Delmastro, “Sensing social interactions through ble beacons and commercial mobile devices,” *Pervasive and Mobile Computing*, vol. 67, p. 101198, 2020.

[3] P. Cassarà, F. Potortì, P. Barsocchi, and M. Girolami, “Choosing an rss device-free localization algorithm for ambient assisted living,” in *2015 International Conference on Indoor Positioning and Indoor Navigation (IPIN)*, 2015, pp. 1–8.

[4] M. Girolami, F. Mavilia, F. Furfari, and P. Barsocchi, “An experimental evaluation based on direction finding specification for indoor localization and proximity detection,” *IEEE Journal of Indoor and Seamless Positioning and Navigation*, vol. 2, pp. 36–50, 2024.

[5] M. Girolami, F. Furfari, P. Barsocchi, and F. Mavilia, “A bluetooth 5.1 dataset based on angle of arrival and rss for indoor localization,” *IEEE Access*, vol. 11, pp. 81 763–81 776, 2023.

[6] M. Girolami, P. Barsocchi, F. Furfari, D. La Rosa, and F. Mavilia, “Evaluation of angle of arrival in indoor environments with bluetooth 5.1 direction finding,” in *2022 18th International Conference on Wireless and Mobile Computing, Networking and Communications (WiMob)*, 2022, pp. 284–289.

[7] M. Qi, B. Xue, and W. Wang, “Calibration and compensation of anchor positions for uwb indoor localization,” *IEEE Sensors Journal*, vol. 24, no. 1, pp. 689–699, 2024.

[8] M. J. Bocus and R. Piechocki, “A comprehensive ultra-wideband dataset for non-cooperative contextual sensing,” *Scientific Data*, vol. 9, no. 1, p. 650, Oct 2022.

[9] A. Khan, T. Farnham, R. Kou, U. Raza, T. Premalal, A. Stanoev, and W. Thompson, “Standing on the shoulders of giants: Ai-driven calibration of localisation technologies,” in *2019 IEEE Global Communications Conference (GLOBECOM)*, 2019, pp. 1–6.

[10] S. Han, H. Yoo, H. Choo, and B.-J. Jang, “Ieee 802.15.4z uwb angle of departure tag design for indoor positioning,” in *2023 53rd European Microwave Conference (EuMC)*. IEEE, 2023, pp. 975–978.

[11] T. Margiani, S. Cortesi, M. Keller, C. Vogt, T. Polonelli, and M. Magno, “Angle of arrival and centimeter distance estimation on a smart uwb sensor node,” *IEEE Transactions on Instrumentation and Measurement*, 2023.

[12] M. Naseri, A. Shahid, G.-J. Gordebeke, S. Lemey, M. Boes, S. Van de Velde, and E. De Poorter, “Machine learning-based angle of arrival estimation for ultra-wide band radios,” *IEEE Communications Letters*, vol. 26, no. 6, pp. 1273–1277, 2022.

[13] M. Heydariaan, H. Dabirian, and O. Gnawali, “Anguloc: Concurrent angle of arrival estimation for indoor localization with uwb radios,” in *2020 16th International Conference on Distributed Computing in Sensor Systems (DCOSS)*. IEEE, 2020, pp. 112–119.